



Faculty of Science  
University of Technology Sydney, Australia

---

# **Modelling and surgical analysis of fracture repair of the facial skeleton using generic and patient matched finite element models**

---

**Richard Conway**

**October 2017**

**This dissertation is submitted for the degree of Doctor of Philosophy**

## **CERTIFICATE OF ORIGINAL AUTHORSHIP**

This thesis is the result of a research candidature conducted jointly with another University as part of a collaborative Doctoral degree. I certify that the work in this thesis has not previously been submitted for a degree nor has it been submitted as part of the requirements for a degree except as part of the collaborative doctoral degree and/or fully acknowledged within the text.

I also certify that the thesis has been written by me. Any help that I have received in my research work and preparation of the thesis itself has been acknowledged. In addition, I certify that all information sources and literature used are indicated in the thesis.

---

**Richard Conway**

---

**Date**

# ACKNOWLEDGEMENT

First and foremost, I express my gratitude to my supervisors, Professor Besim Ben-Nissan and Professor Bruce Milthorpe, for sharing their knowledge and passion for this subject during the research work, for contributing significantly to my professional growth and finally for their friendship.

Whilst this research thesis is novel, it draws from previous works to understand where finite element analysis began to where it is currently, as well as its limitations to date, particularly in the fields of medicine and dentistry. In particular, I have drawn extensively on the technical expertise of my academic colleagues so that I could provide my surgical expertise to produce this work. As such special acknowledgement goes to the following:

Dr Andrew Choi has been invaluable for his friendship, guidance and expertise in preparing this thesis. In particular, he helped me understand finite element models and assisted me in the technical aspects of preparing and interpreting generic finite element models used in this thesis, which was fundamental in completing the research.

Dr Valerio Taraschi helped immensely in all aspects of the preparation and interpretation of the patient specific model.

Professors Ben-Nissan and Milthorpe allowed me to understand the previous and current works of Drs Choi and Taraschi. In doing so, the foundations to produce this thesis were formed.

Mr Richie Mohan from Medical and Optical provided invaluable data relating to commercially available plating systems that were incorporated into this analysis.

I would like to thank my family for supporting me through this long process and providing invaluable encouragement. With all my heart, thank you Danya, Amelia and Charlotte.

Last but not least I would like to thank Lei Cameron who helped me in proofreading and formatting my thesis, as well as providing valuable insight into my preparation of this document.

## **PREFACE**

As a surgeon working in the maxillofacial field I have always had a keen interest in trauma of the facial skeleton. As part of my contact at the University of Technology with Professor Ben-Nissan, Professor Milthorpe, Dr Choi and Dr Taraschi over the past 20 years I have had the honour of being involved in finite element based research. During this time, it became apparent that utilising this methodology to analyse both current fracture management and future directions of fracture management was a worthy ground for research as part of a doctorate of philosophy. To achieve this goal, I have been most fortunate to have the wealth of technical knowledge from my aforementioned university colleagues to draw upon and integrate into my surgical expertise.

The following dissertation presents my analysis as a surgeon of modelling and fracture repair of the facial skeleton, using generic and patient matched finite element models with technical support provided by those academic colleagues addressed in my acknowledgements.

I hope that those who read this thesis, whether scientists or clinicians or both, find it as interesting as I have.

# TABLE OF CONTENTS

<b>CERTIFICATE OF ORIGINAL AUTHORSHIP</b>	<b>I</b>
<b>ACKNOWLEDGEMENT</b>	<b>II</b>
<b>PREFACE</b>	<b>III</b>
<b>TABLE OF CONTENTS</b>	<b>IV</b>
<b>LIST OF FIGURES</b>	<b>IX</b>
<b>LIST OF TABLES</b>	<b>XIX</b>
<b>PUBLICATIONS ARISING FROM RESEARCH WORK</b>	<b>XXII</b>
<b>ABSTRACT</b>	<b>XXIII</b>
<b>ABBREVIATIONS</b>	<b>XXVI</b>
<b>CHAPTER 1: INTRODUCTION</b>	<b>1</b>
1.1 Approach	1
1.2 History and the understanding of trauma as it contributes to our current practice	1
1.3 Fracture of the mandible and surgical aspects	9
1.4 Rapid repair and recovery from facial fractures	13
1.5 Rigid versus semi-rigid fixation, micromovement and stress shielding	19
1.6 Limitations of current fracture management	20
1.7 Specific difficulties with the fractured edentulous mandible	25
1.8 Anticipation of research and its application	26
<b>CHAPTER 2: ANATOMY AND BIOMECHANICS OF THE MANDIBLE</b>	<b>28</b>
2.1 Anatomy of the mandible	28
2.1.1 Major muscles of mastication	29
2.1.2 Accessory muscles of mastication	31
2.1.3 The temporomandibular joint complex	34
2.2 Biomechanics of the mandible	36
2.2.1 Non-lever action hypotheses	38
2.3 Biomechanics of mandibular movement	39
2.3.1 Biomechanics of the Temporomandibular Joint	39
2.3.2 Mastication biomechanical analysis	41
2.3.3 The chewing stroke	41
2.3.4 Tooth contacts during mastication	42

2.3.5	Forces of mastication	43
<b>2.4</b>	<b>Mandibular movement</b>	<b>43</b>
2.4.1	Mandibular rest position	44
2.4.2	Opening movement	44
2.4.3	Protrusive mandibular movement	45
2.4.4	Laterotrusive mandibular movement	46
2.4.5	Retrusive mandibular movement	47
2.4.6	Closing movement	47
<b>2.5</b>	<b>Biomechanics and anatomy of the edentulous mandible</b>	<b>48</b>
2.5.1	Anatomy of the edentulous mandible	48
2.5.1.1	<i>Lack of teeth</i>	48
2.5.1.2	<i>Loss of alveolar bone</i>	48
2.5.1.3	<i>Alteration in mandibular blood supply</i>	48
2.5.2	Edentulous bite force	50
2.5.3	Edentulous chewing stroke	50
<b>CHAPTER 3:</b>	<b>FINITE ELEMENT MODEL OF THE HUMAN MANDIBLE</b>	<b>52</b>
3.1	What is a finite element model?	52
3.2	Complexity of exterior shape and interior structure of the mandible	53
3.3	Influence of the morphological complexity on the modelling	55
3.4	Cortical bone property variations	56
3.5	Cancellous bone property variations	57
3.6	Interface between bone types	60
3.7	Choice of material properties	62
3.8	Biomechanical considerations	62
<b>CHAPTER 4:</b>	<b>FIRST OUTPUT – MODELLING OF AN AVERAGE EDENTULOUS HUMAN MANDIBLE</b>	<b>64</b>
4.1	Introduction	64
4.2	The first model	64
4.3	Equipment used	65
4.3.1	STRAND7	65
4.3.2	Digitiser	66
4.3.3	Earlier models	66
4.4	Forces acting on the mandible	72
4.4.1	Clenching	76
4.4.2	Opening	77
4.4.3	Protrusion	80
4.5	Summary	82
<b>CHAPTER 5:</b>	<b>SECOND OUTPUT – PATIENT SPECIFIC MODELLING</b>	<b>84</b>
5.1	Mandibular model	85

<b>5.2</b>	<b>Biomechanical Approach and FEA</b>	<b>86</b>
<b>5.3</b>	<b>FEM models and differentiation criteria: Materials, restraints Hounsfield units and data acquisition</b>	<b>87</b>
<b>5.4</b>	<b>FEA model: Biomechanical considerations</b>	<b>92</b>
5.4.1	Material mapping	92
5.4.2	Load application	93
5.4.3	Equilibria and the reaction force	93
5.4.4	Reaction force positioning	95
5.4.5	Finite element analysis application	97
<b>CHAPTER 6: RESULTS AND DISCUSSION OF THE COMPARISON BETWEEN THE GENERIC MODEL AND PATIENT SPECIFIC MODEL</b>		<b>99</b>
<b>6.1</b>	<b>Introduction</b>	<b>99</b>
<b>6.2</b>	<b>The generic model (MI)</b>	<b>101</b>
<b>6.3</b>	<b>The patient specific model (MII)</b>	<b>106</b>
<b>CHAPTER 7: THIRD OUTPUT – MANDIBULAR FRACTURE AND REPAIR MODELLING METHOD</b>		<b>112</b>
<b>7.1</b>	<b>Introduction</b>	<b>112</b>
<b>7.2</b>	<b>Fracture model of the mandible</b>	<b>113</b>
<b>7.3</b>	<b>Constants within the various analyses</b>	<b>118</b>
7.3.1	Linear plate dimensions	118
7.3.2	Placement of fracture plates	118
7.3.3	Material properties data	118
<b>7.4</b>	<b>Design of the fracture fixation systems to be analysed</b>	<b>120</b>
7.4.1	Linear plate varying screw hole diameter	121
7.4.2	Linear plate varying thickness	122
7.4.3	Linear plate varying material (Ti-6Al-4V, PLA and ZrO <sub>2</sub> )	122
7.4.5	Mesh plate design	123
<b>7.5</b>	<b>Description of each analysis for design variations</b>	<b>125</b>
7.5.1	Variation in old versus new fracture site for a 1.0mm thick Ti-6Al-4V plate with 2.25mm diameter screw holes under the functional movement of clenching (measuring von Mises stress)	125
7.5.2	Variation in functional movements of clenching, opening and protrusion for a 1.0mm thick Ti-6Al-4V linear plate with 2.25mm diameter holes (measuring von Mises stress and distortion)	125
7.5.3	Variation in screw hole diameter of a Ti-6Al-4V linear fracture plate under the functional movements of opening, protrusion and clenching (measuring von Mises stress and distortion)	125
7.5.4	Variation of a Ti-6Al-4V plate with thicknesses of 0.5mm, 1.0mm and 2.0mm respectively under the functional movement of clenching, with screw hole diameter constant at 2.25mm (measuring von Mises stress and distortion)	126

7.5.5	Variations in plate material, Ti-6Al-4V, PLA and ZrO <sub>2</sub> under the functional movement of clenching with plate thickness and screw hole diameter being constant at 1.0mm and 2.25mm respectively (measuring von Mises stress and distortion)	126
7.5.6	Variation in a linear laminated fracture plate (measuring von Mises stress and distortion)	126
7.5.7	Variation in a mesh fracture plate (measuring von Mises stress and distortion)	127
7.5.8	Application of linear design plate across a fracture in the patient specific model (measuring von Mises stress and distortion)	127
7.7	<b>Measurement criteria for data collection and presentation</b>	<b>129</b>

## **CHAPTER 8: THIRD OUTPUT – MANDIBULAR FRACTURE AND REPAIR MODELLING RESULTS** **133**

8.1	<b>Results for variation in old versus new fracture site for a 1.0mm thick Ti-6Al-4V plate with 2.25mm diameter screw holes in clenching</b>	<b>133</b>
8.2	<b>Results for variation in functional movements of clenching, opening and protrusion for a 1.0mm thick Ti-6Al-4V plate with 2.25mm diameter screw holes measuring for each scenario von Mises stress and distortion.</b>	<b>135</b>
8.2.1	Effects of functional movements on von Mises stress	135
8.2.2	Effects of functional movements on distortion	138
8.3	<b>Results for variation in a 1.0mm thick Ti-6Al-4V plate with screw hole diameters of 0.62mm, 1.25mm, 1.88mm and 2.25mm under the functional movement of clenching measuring maximum von Mises stress and distortion</b>	<b>141</b>
8.3.1	Results for 0.62mm hole diameter plate, maximum von Mises stress and distortion	141
8.3.2	Results for 1.25mm hole diameter plate, maximum von Mises stress and distortion	142
8.3.3	Results for 1.88mm screw hole diameter plate, maximum von Mises stress and distortion during the functional movement of clenching	143
8.3.4	Results for 2.25mm screw hole diameter plate, maximum von Mises stress and distortion during the functional movement of clenching	144
8.3.5	Cumulative tabulation and graph plot of results	144
8.4	<b>Results for von Mises stress and distortion in the variation of a Ti-6Al-4V plate with thicknesses of 0.5mm, 1.0mm and 2.0mm respectively under the functional movement of clenching with screw hole diameter constant at 2.25mm</b>	<b>146</b>
8.4.1	Results for 0.5mm thick plate	146
8.4.2	Results for 1.0mm thick plate	146
8.4.3	Results for 2.0mm thick plate	147



8.4.4	Tabulation and graph plot of results from the fracture segment	148
8.4.5	Significant points of the data results	149
<b>8.5</b>	<b>Results for von Mises stress and distortion with variation in plate material, Ti-6Al-4V, PLA and ZrO<sub>2</sub> under the functional movement of clenching.</b>	<b>151</b>
8.5.1	Results for Ti-6Al-4V	151
8.5.2	Results for PLA	151
8.5.3	Results for ZrO <sub>2</sub>	152
<b>8.6</b>	<b>Results for von Mises stress and distortion with variation in a composite laminated plate (Ti-6Al-4V and PLA) under the functional movement of clenching</b>	<b>153</b>
8.6.1	Results for PLA laminate facing outwards	154
8.6.2	Results for Ti-6Al-4V laminate facing outwards	155
<b>8.7</b>	<b>Results for variation in mesh fracture plate in clenching</b>	<b>157</b>
<b>8.8</b>	<b>Results from application of linear design plate across a fracture in the patient specific model during clenching</b>	<b>159</b>
<b>8.8</b>	<b>Summation and tabulation of all data set results</b>	<b>160</b>
<b>CHAPTER 9: SUMMARY AND CONCLUSIONS</b>		<b>163</b>
<b>CHAPTER 10: PROPOSED FUTURE WORK</b>		<b>184</b>
<b>APPENDIX A: TRANSLATION OF CT DENSITY (HOUNSFIELD UNITS) INTO A FINITE ELEMENT MODEL</b>		<b>186</b>
1	Introduction	186
2	Why chose an edentulous model?	186
3	Relation between the Hounsfield unit and density	187
4	Mapping density and elasticity	194
<b>APPENDIX B: CT NUMBERS DENSITY, E FREQUENCY AND DISTRIBUTION IN MODEL MII</b>		<b>197</b>
<b>BIBLIOGRAPHY</b>		<b>204</b>

# LIST OF FIGURES

## Abstract

Figure 0.1	Facial skeleton affected by congenitally associated tooth absence and neoplasia, requiring complex reconstruction with dental implants, grafting and fixation plate.....	xxv
------------	--	-----

## Chapter 1

Figure 1.1	Mean length of stay in days for injury by age and sex, Australia, 2012-13 (Australian Institute of Health and Welfare).....	4
Figure 1.2	Flowchart of trauma by anatomical region that shows where facial trauma lies within the spectrum.....	6
Figure 1.3	Incidence of facial bone fractures (VandeGriend, 2015) .....	8
Figure 1.4	Facial bone fractures requiring surgical repair (VandeGriend, 2015).....	8
Figure 1.5	Intermaxillary wire fixation (modified, courtesy of AO Foundation).....	10
Figure 1.6	External fixators used in managing facial trauma from gunshot wound .....	11
Figure 1.7	Inadequate fracture apposition and fixation leading to persistent fracture displacement and delayed healing.....	12
Figure 1.8	Inadequate fracture fixation leading to implant failure resulting in fracture non-union in an elderly female with osteoporosis and an atrophic mandible .....	12
Figure 1.9	Four stages of fracture healing: (a) haematoma formation; (b) bone regeneration; (c) bony callous formation; and (d) bone remodelling (courtesy of Boundless).....	17
Figure 1.10	Gap discontinuity in repaired fractured mandible despite immobilisation fracture healing not occurring.....	18
Figure 1.11	Lane's metal plate introduced in 1895 but abandoned due to corrosion .....	21
Figure 1.12	Example of contemporary four screw hole Ti miniplates .....	22
Figure 1.13	Failed commercially pure Ti plate for osteosynthesis (Azevedo, 2003).....	23
Figure 1.14	FEM of four hole miniplate showing the location of highest von Mises stress (Sugiura, 2009).....	24

Figure 1.15	Plate benders used to manipulate a generic non-patient specific plate .....	24
Figure 1.16	Diagram showing Luhr Class III atrophy and a common clinical presentation of bilateral fractures (courtesy of AO Foundation).....	26
<b>Chapter 2</b>		
Figure 2.1	Showing the vertical ramus joining with the horizontal ramus at the angle of the mandible and alveolar bone at the superior aspect of the horizontal ramus housing the dentition (diagram constructed using 3D4MEDICAL software) .....	29
Figure 2.2	Showing the masseter in isolation above and its combination with the medial pterygoid muscle to form the pterygo-masseteric sling (diagram constructed using 3D4MEDICAL software) .....	30
Figure 2.3	Temporalis muscle (diagram constructed using 3D4MEDICAL software) .....	31
Figure 2.4	Lateral pterygoid muscle (diagram constructed using 3D4MEDICAL software) .....	32
Figure 2.5	Digastric muscle is a depressor of the mandible in the chewing cycle (diagram constructed using 3D4MEDICAL software).....	33
Figure 2.6	Geniohyoid muscle is a depressor of the mandible in the chewing cycle (diagram constructed using 3D4MEDICAL software).....	33
Figure 2.7	Bony components of the temporomandibular joint (diagram constructed using 3D4MEDICAL software).....	34
Figure 2.8	Soft tissue component of the temporomandibular joint (Netter Atlas of Human Anatomy).....	35
Figure 2.9	Mandible as a Class III lever (Smith, 1978).....	36
Figure 2.10	Demonstrates the inferior joint cavity and superior joint cavity (Lumen, Anatomy of Selected Synovial Joints).....	40
Figure 2.11	Illustrates temporomandibular rotation and translation (Neumann, 2016).....	40
Figure 2.12	The chewing stroke (Croll 2017).....	41
Figure 2.13	Protrusive mandibular movement showing occlusal contacts (Okeson, 1985) .....	45
Figure 2.14	Left laterotrusive movement (Okeson, 1985).....	46

Figure 2.15	Retrusive mandibular movement showing occlusal contacts (Okeson, 1985) .....	47
Figure 2.16	Inferior alveolar artery which provides the dentate mandible with blood supply (diagram constructed using 3D4MEDICAL software).....	49
<b>Chapter 3</b>		
Figure 3.1	Morphologically different bone samples acquired from female and male mandibles .....	54
Figure 3.2	Stress profiles along bone-implant interface with varying thickness assigned to the cortical bone (Guan et al., 2009) .....	59
Figure 3.3	Example of segmentation using a ‘threshold’ function (modified from Taraschi, 2016) .....	60
Figure 3.4	Examples of cortical-cancellous bone model approximation prepared in Amira and visualised in ANSYS software (modified from Taraschi, 2016) .....	61
Figure 3.5	Significant artefact from metallic restorations in a mandibular CT scan (Tohnak, 2011) .....	61
<b>Chapter 4</b>		
Figure 4.1	A typical cross-section of the human mandible showing 28 vertical sections (modified from Ben-Nissan et al., 1987).....	66
Figure 4.2	Element divisions (modified from Ben-Nissan et al., 1987).....	67
Figure 4.3	Nodal point generation using digitizer (modified from Ben-Nissan et al., 1987).....	68
Figure 4.4	A typical cross-section of the mandible generated from nodal points (produced in STRAND7 modified from Choi et al., 2005).....	69
Figure 4.5	Finite element model of the human mandible (produced in STRAND7 modified from Choi et al., 2005).....	69
Figure 4.6	Finite element and wire frame mandibular models: The cortical bone outline is represented in orange and the cancellous bone inner layer is represented in blue (produced in STRAND7 modified from Choi et al., 2005) .....	70
Figure 4.7	Frontal and lateral views of the finite element model of the human mandible, showing restraining spring elements (produced in STRAND7 modified from Choi et al., 2005).....	71
Figure 4.8	Lateral projection of muscle force directions (diagram constructed using 3D4MEDICAL software) .....	75

Figure 4.9	Diagrammatic representation of direction of muscle pull during clenching (diagram constructed using 3D4MEDICAL software).....	76
Figure 4.10	Applied muscle, joint reaction and bite forces and coordinate system during clenching (modified from Choi, 2004) .....	77
Figure 4.11	Diagram of interplay between FD and FLT to produce moment arm and opening of the mandible (constructed using 3D4MEDICAL software).....	78
Figure 4.12	Applied muscle and joint reaction forces and coordinate system during opening (modified from Choi, 2005) .....	80
Figure 4.13	Diagram of interplay between FMP and FLT to produce gliding and protrusion of the mandible (constructed using 3D4MEDICAL software).....	81
Figure 4.14	Applied muscle and joint reaction forces and coordinate system during protrusion (modified from Choi, 2005).....	82
<b>Chapter 5</b>		
Figure 5.1	Process in conducting surgical analysis of a patient specific finite element model .....	85
Figure 5.2	Three-dimensional vector representation of loads applied during clenching including joint reactions forces (modified from Taraschi, 2016).....	94
Figure 5.3	Variable area for reaction force application during clenching simulation (SolidWorks Educational Edition, c. 1195-2008, Dassault Systemes©).....	96
<b>Chapter 6</b>		
Figure 6.1	Representation of results obtained by Choi et al. (2005) for von Mises stresses .....	101
Figure 6.2	Probing of the equivalent stress in the molar region (modified from Taraschi, 2016).....	101
Figure 6.3	Example of deformation colour bands for visualising the simulation results (modified from Taraschi, 2016) .....	102
Figure 6.4	Deformation during clenching (modified from Taraschi, 2016).....	103
Figure 6.5	Deformation during wide opening (modified from Taraschi, 2016).....	103
Figure 6.6	Erroneous von Mises stress maximum during clenching (modified from Taraschi, 2016) .....	105

Figure 6.7	Erroneous von Mises stress maximum during clenching (modified from Taraschi, 2016) .....	105
Figure 6.8	Colour bands corresponding to deformation during clenching (scalar values are in micrometers) (results post-processed with ANSYS APDL; modified from Taraschi, 2016) .....	107
Figure 6.9	Results for deformation during clenching visualised in ANSYS Workbench Mechanical (modified from Taraschi, 2016) .....	108
Figure 6.10	von Mises stress in premolar regions during clenching (units are MPa) (modified from Taraschi, 2016).....	108
Figure 6.11	von Mises stress during clenching showing higher stresses on the coronoid processes (units are MPa) (modified from Taraschi, 2016) ...	109
Figure 6.12	Deformed shape (coloured blue) versus undeformed shape during wide opening movement (modified from Taraschi, 2016).....	109
Figure 6.13	Mandibular distortion during wide opening movement (units are in Pa) (modified from Taraschi, 2016) .....	110
Figure 6.14	Colour bands corresponding to deformation during wide opening (values are in micrometers) (modified from Taraschi, 2016).....	110
Figure 6.15	von Mises stress during wide opening (units are Pa) (results post-processed in ANSYS APDL; modified from Taraschi, 2016) .....	111
<b>Chapter 7</b>		
Figure 7.1	Finite element wire frame mandible model (produced in STRAND7) (modified from Choi, 2005) .....	114
Figure 7.2	Location of the original section before reconstruction on the mandible model (modified from Choi, 2005).....	114
Figure 7.3	Location of the original section after reconstruction on the mandible model (modified from Choi, 2005).....	115
Figure 7.4	Section after reconstruction: (A) three-dimensional view; (B) top view (produced in STRAND7 modified from Choi, 2005).....	115
Figure 7.5	Location and modelling of the fracture site is shown by the arrows (modified from Choi 2005) .....	116
Figure 7.6	Three-dimensional FEM and analysis showing the distortion (top and middle) and compressive stresses (bottom figure) of the mandible under biting conditions (modified from Choi, 2005) .....	117
Figure 7.7	FEM of the fractured mandible with fixation plate (produced in STRAND7).....	119

Figure 7.8	Modelling of the fracture plates with various screw hole diameters.....	121
Figure 7.9	Composite laminate design with the Ti-6Al-4V side facing outwards followed by the reverse with the PLA laminate facing outwards .....	123
Figure 7.10	Comparison of mesh design to ‘traditional’ linear plate design.....	124
Figure 7.11	Model with a new design Ti-6Al-4V mesh plate applied across fracture at the angle of the mandible .....	124
Figure 7.12	Linear fracture plate modelled in Autodesk inventor.....	127
Figure 7.13	Assembled model ready for analysis with scale for reference to dimensions.....	128
Figure 7.14	Depth, direction and location of measurements perpendicular to plate surface.....	129
Figure 7.15	Three key points in data measurement for FS, starting from the outer surface of the plate to the centre of the medullary cavity .....	130
Figure 7.16	FEM Ti-6Al-4V linear plate in situ in the FS of the overall fixation system model (plate = 19.5mm long x 1.0mm thick x 3.0mm wide with 2.25mm diameter screw holes).....	131
Figure 7.17	FEM plate extracted from the overall model and presented in isolation .....	131
<b>Chapter 8</b>		
Figure 8.1	(A & B) Stress analysis for ‘old’ and ‘new’ fractures.....	133
Figure 8.2	von Mises stress curves for FS of ‘old’ and ‘new’ fractures.....	134
Figure 8.3	FEM of the IP showing areas of maximum stress concentration in pink during clenching.....	136
Figure 8.4	FEM of IP during the functional movement of opening (maximum stress reached is highlighted in FEM models as pink colouration).....	136
Figure 8.5	FEM of IP during the functional movement of protrusion (maximum stress is illustrated by pink colouration) .....	137
Figure 8.6	Graph plot for FS – comparison for clenching, opening and protrusion with peaks stress of 122MPa, 70MPa and 81MPa respectively.....	137
Figure 8.7	FEM of IP for distortion during functional movement of clenching.....	138
Figure 8.8	FEM of IP for distortion during functional movement of opening .....	139

Figure 8.9	FEM of IP for distortion during functional movement of protrusion....	139
Figure 8.10	FEM of IP and concentration of point of maximum von Mises stress at ends of the plate (coloured pink) .....	141
Figure 8.11	FEM of IP and concentration of point of maximum distortion at the proximal end of the plate (coloured pink) .....	142
Figure 8.12	FEM of IP. Maximum stress concentrated at ends of the plate (coloured pink) .....	142
Figure 8.13	FEM of IP. Maximum distortion in the FEM (coloured pink) .....	143
Figure 8.14	FEM of IP. Maximum von Mises stress (coloured pink) .....	143
Figure 8.15	FEM of IP. Maximum distortion (coloured pink) .....	144
Figure 8.16	Graph plot of von Mises stress of FS from plate surface through to mandibular cortical and cancellous bone .....	145
Figure 8.17	FEM of IP with thickness of 0.5mm (area of maximum stress concentration coloured pink) .....	146
Figure 8.18	FEM of IP with thickness of 1.0mm (area of maximum stress concentration coloured pink) .....	147
Figure 8.19	FEM of IP with thickness of 2.0mm (area of maximum stress concentration coloured pink) .....	147
Figure 8.20	Graph plot showing FS variation in von Mises stress for plates with thicknesses of 0.5mm, 1.0mm and 2.0mm, measured from the plate surface through to mandibular cortical and cancellous bone .....	148
Figure 8.21	Graph plot showing FS variation of distortion .....	149
Figure 8.22	FEM of IP for PLA plate showing maximum stress concentration as illustrated by pink colouration .....	151
Figure 8.23	FEM of isolated plate for ZrO <sub>2</sub> plate showing maximum stress concentration as illustrated by pink colouration .....	152
Figure 8.24	Graph plot of FS data for von Mises stress with Ti-6Al-4V, PLA and ZrO <sub>2</sub> plates .....	152
Figure 8.25	Graph plot of distortion within the FS .....	153
Figure 8.26	Composite laminate design with Ti-6Al-4V side facing outwards followed by the reverse with PLA laminate facing outwards .....	154
Figure 8.27	FEM of IP for composite laminated with PLA laminate facing outward .....	155



Figure 8.28	FEM of IP for composite laminated with Ti laminate facing outward .....	155
Figure 8.29	Graph plot of FS data for von Mises stress with composite laminate plates .....	156
Figure 8.30	Graph plot of distortion of the FS.....	156
Figure 8.31	FEM of IP for Ti mesh showing maximal stress of 88.86MPa illustrated by areas of pink colouration .....	157
Figure 8.32	FEM of IP for Ti mesh showing maximal distortion of 0.0867mm.....	157
Figure 8.33	Comparison in performance between mesh plate and linear plate design (19.5mm x 3.0mm x 1.0mm with 2.25mm diameter holes) for von Mises stress in the FS.....	158
Figure 8.34	FEM of IP tested for von Mises stress during clenching (mandibular model is greyed out to emphasise the plate) .....	159
Figure 8.35	FEM of IP tested for distortion during clenching (mandibular model is greyed out to emphasize the plate and a scale is provided to reference for dimensions).....	160

## Chapter 9

Figure 9.1	Shows inadequate fracture fixation leading to fixation system failure resulting in fracture non-union in an elderly female with osteoporosis and an atrophic mandible.....	163
Figure 9.2	Incidence of facial bone fractures (VandeGriend, 2015) .....	164
Figure 9.3	Facial bone fractures requiring surgical repair (VandeGriend, 2015)...	164
Figure 9.4	Four stages of fracture healing: (i) haematoma formation; (ii) bone regeneration; (iii) bony callous formation; and (iv) bone remodelling (courtesy of Boundless).....	166
Figure 9.5	Plate benders being applied to manipulate and shape a Ti plate prior to insertion onto the fracture site, producing material distortion at the site where plate failure is most likely to occur (courtesy of AO Foundation).....	167
Figure 9.6	FEM of four screw hole miniplate showing the location of highest von Mises stress (Sugiura, 2009).....	167
Figure 9.7	Failed commercially pure Ti plate for osteosynthesis (Azevedo, 2003).....	167
Figure 9.8	FEM of bridge C section beam (courtesy of Vanderbilt University School of Engineering).....	169

Figure 9.9	Summary of six data set results .....	171
Figure 9.10	Showing comparison in stress curve for ‘old’ generic model and ‘new’ generic model .....	174
Figure 9.11	Graph plot of von Mises stress from plate surface through to mandibular cortical and cancellous bone .....	176
Figure 9.12	Graph plot showing variation in von Mises stress for plates with thicknesses of 0.5mm, 1.0mm and 2.0mm measured from the plate surface through to mandibular cortical and cancellous bone .....	177
Figure 9.13	Graph plot of FS data for von Mises stress with Ti-6Al-4V, PLA and ZrO <sub>2</sub> plates .....	178
Figure 9.14	Graph plot of FS data for von Mises stress with composite laminate plates.....	179
Figure 9.15	Comparison of the seven available screw hole in the linear plate design versus the twenty available in the mesh plate design.....	180
Figure 9.16	Comparison in performance between mesh plate and linear plate design (19.5mm x 3.0mm x 1.0mm with 2.25mm diameter screw holes) for von Mises stress .....	181

## Chapter 10

Figure 10.1	Mandibular FEM with muscle forces, fracture and fixation bar .....	185
Figure 10.2	Showing close up of fracture and fixation bar.....	185

## Appendix A

Figure A.1	CT numbers correspondent to water are averaged over the scanned volume of a little water balloon (here circled in yellow) kept in the patient’s mouth (modified from Taraschi, 2016) .....	188
Figure A.2	Mesh in Bonemat Young’s modulus (modified from Taraschi, 2016).....	196

## Appendix B

Figure B.1	CT numbers frequency showing distribution of CT numbers in the patient selective mandibular mesh (modified from Taraschi, 2016).....	197
Figure B.2	Frequency of Young’s modulus in the mandibular mesh (modified from Taraschi, 2016) .....	198
Figure B.3	Relation between CT numbers and density (modified from Taraschi, 2016) .....	200

Figure B.4	<i>Bonemat</i> graphical user interface showing all the parameters used to generate the conversion from CT numbers to Young's modulus for a specific finite element mesh (modified from Taraschi, 2016).....	201
Figure B.5	Density distribution showing frequency of calculated densities in the mandibular mesh (modified from Taraschi, 2016).....	202
Figure B.6	Distribution of Young's modulus in the finite element mesh calculated using an inverse approach (modified from Taraschi, 2016).....	202

# LIST OF TABLES

## Chapter 1

Table 1.1	Major external cause groups for injury cases, by sex, Australia, 2012-2013 (Australian institute of Health and Welfare).....	2
Table 1.2	Trends in age standardised rates of injury cases by type of external cause, Australia, 1999-2000 to 2012-2013 (Australian Institute of Health and Welfare, 2015) .....	3
Table 1.3	Cost in US\$ for hospitalisation to repair various facial fractures (Allareddy) .....	7
Table 1.4	Luhr's classification for fractures of the edentulous atrophic mandible .....	25

## Chapter 3

Table 3.1	Summary of various Young's modulus values for dry cortical bone.....	56
Table 3.2	Mechanical properties measured for femoral cortical bone by different studies .....	56
Table 3.3	Relation between mechanical properties of the cortical bone and subjects showing comparison of different studies.....	57
Table 3.4	Cody's results (1996) for range of femoral cancellous bone mechanical properties .....	58
Table 3.5	Summary of material property values used in this thesis for cortical and cancellous bone.....	62
Table 3.6	Reference system used for the FEM.....	63

## Chapter 4

Table 4.1	Physiological cross-sectional area ( $\text{cm}^2$ ) of the facial muscles .....	73
Table 4.2	Average maximum muscle tension ( $\Gamma$ ) in $\text{N/m}^2$ .....	73
Table 4.3	Averaged calculated maximum muscle forces (N) in each single muscle group and related standard deviations.....	74
Table 4.4	Calculated muscle, joint reaction and bite force magnitudes (N) acting on the mandible during clenching (Ben-Nissan, 1987) .....	74
Table 4.5	Calculated muscle and joint reaction force magnitudes (N) acting on the mandible during opening (Ben-Nissan, 1987).....	79

Table 4.6	Calculated muscle and joint reaction force magnitudes (N) acting on the mandible during protrusion (Ben-Nissan, 1987) .....	80
<b>Chapter 5</b>		
Table 5.1	Comparative values of Hounsfield units (Shetty et al., 2009; Choi et al., 2010) .....	91
<b>Chapter 6</b>		
Table 6.1	Maximum von Mises stresses recorded during functional movements in Choi et al(2005) .....	100
Table 6.2	Results for maximum distortion in the first and second molar region during clenching and wide opening movement compared with previous investigations .....	104
Table 6.3	Results for maximum von Mises stress in the first and second molar region during clenching and wide opening movement. ....	106
Table 6.4	Results for mandibular deformation of the MII model during wide opening compared with values obtained in the MI model .....	107
Table 6.5	Results for mandibular deformation of the MII model during clenching compared with values obtained in the MI model .....	107
<b>Chapter 7</b>		
Table 7.1	Mechanical properties used in finite element computations .....	120
Table 7.2	Mechanical properties of the fracture plates used in this study.....	120
<b>Chapter 8</b>		
Table 8.1	Comparison of highest stress and distortion values between clenching and protrusion/opening .....	140
Table 8.2	Comparison of variation in results with increasing screw hole diameter during clenching .....	144
Table 8.3	Comparison of variations in results with increasing plate thickness as maximum stress and distortion is affected within the fracture segment.....	148
Table 8.4	Comparison of cross sectional area between mesh plate linear plate design (19.5mm x 3.0mm x 1.0mm) varying hole diameter from 2.25mm to 0.62mm.....	158
Table 8.5	Summation of data set results.....	161

## Chapter 9

Table 9.1	Results for seven data sets .....	172
-----------	-----------------------------------	-----

## Appendix A

Table A.1	Relationship between Hounsfield units (CT units) and density $\rho$ ( $Kgm^3$ ) for specimens from cancellous bone from different anatomical locations (Rho, 1995) .....	188
Table A.2	Modulus-density relationships according to studies published in literature (Helgason et al., 2008) .....	190
Table A.3	Experimental relationships between elastic modulus and strain rates...	191

## Appendix B

Table B.1	Comparison of stress values obtained for cortical and cancellous bone respectively when using Keller's empirical law and the finite element simulation object of this study .....	203
-----------	---	-----

## PUBLICATIONS ARISING FROM RESEARCH WORK

A.H. Choi, B. Ben-Nissan, R.C. Conway, & I.J. Macha (2104). *Advances in calcium phosphate nanocoatings and nanocomposites*. Advances in Calcium Phosphate Biomaterials, Springer Publishing, pp. 485-511.

A.H. Choi, B. Ben-Nissan, & R.C. Conway (2014). Finite Element Analysis (FEA) in Dentistry. In *Handbook of Oral Biomaterials*, J.P. Matinlinna (Ed.), Singapore: Pan Stanford Publishing, Ch. 17, pp. 535-576.

A.H. Choi, B. Ben-Nissan, & R.C. Conway (2005). Three-dimensional modelling and finite element analysis of the human mandible during clenching. *Australian Dental Journal*, 50(1), 42-48.

A.H. Choi, J.P. Matinlinna, R.C. Conway, & B. Ben-Nissan (2012). Application of Biomaterials and Finite Element Analysis (FEA) in Nanomedicine and Nanodentistry. In: *Computational Finite Element Methods in Nanotechnology*, S.M. Musa (Ed.), CRC Press-Taylor and Francis Group, USA, Ch. 11, pp. 373-399.

A.H. Choi, R.C. Conway, & B. Ben-Nissan (2004). Finite element analysis of ceramic dental implants incorporated into the human mandible, *Key Engineering Materials*, 254, 707-712.

A.H. Choi, R.C. Conway, V. Taraschi, & B. Ben-Nissan (2014). Biomechanics and functional distortion of the human mandible, *Journal of Investigative and Clinical Dentistry*, 6(4), 241-251.

A.H. Choi, B. Ben-Nissan, J.P. Matinlinna, & R.C. Conway (2013). Current perspectives: Calcium phosphate nanocoatings and nanocomposite coatings in dentistry. *Journal of Dental Research*, 92(10), 853-859.

## **ABSTRACT**

### **Surgical analysis of fracture repair of the facial skeleton using generic and patient matched finite element models**

This thesis is aimed at finite element modelling of the fractured and repaired facial skeleton, specifically the mandible and surgical aspects that influence a rapid and complete recovery process without complications that otherwise lead to significant patient morbidity and sometimes mortality.

The mandible, as a site of specific investigation, was chosen due to the following factors. Firstly, as a prominent part of the facial skeleton, the mandible is a highly complex structure, being composed in its hard tissue elements by cancellous and cortical bone and the dental complex consisting of enamel, dentine and cementum. These hard tissue components house the associated soft tissues consisting of major nerves and blood vessels, fat and other connective tissues. Already one can see the complexity of the mandible but its unique anatomical character does not stop there as the entire structure articulates with the remainder of the facial skeleton via the temporomandibular joints.

The mandible is also unique because it is being commonly affected by all of the major disease classifications, being congenital, traumatic, neoplastic, infective, inflammatory and iatrogenic disease. As a consequence, clinicians ranging from dentists through to maxillofacial surgeons are often confronted with complex disease patterns that require complex reconstructive methods to restore form and function (Figure 0.1). At the terminus of reconstruction, these elements of form (cosmesis) and function (speech, facial expression, mastication, deglutition, taste and airway maintenance) are what our patients demand and should be entitled to expect from modern day surgical techniques.

The aim of this work is to look at the fractured mandible using finite element modelling and ascertain what provides the surgeon with the best results when performing



osteosynthesis of the fracture and hence lead to rapid, complete and complication free healing.

The models used in this thesis are based on a well established and validated model, initially taking its heritage from the works of Ben-Nissan in 1987, followed by Choi in 2005. In this thesis, it is termed the 'generic (GEN) model'. A second model is also used throughout this thesis, which is based on computed tomography scans of a human mandible, termed as the 'patient specific (PS) model'. With the GEN and PS models, various fracture fixation systems were designed and applied to both FE models and analysed for their efficacy. This brings to the study a unique attribute of comparing a GEN model with a PS model, thus allowing multiple fracture fixation systems to be analysed. In doing so, a better correlation is provided with the pathophysiology and mechanics of trauma as it occurs in vivo.

The results of this study show that most importantly we have been able to produce a valid models that closely mirrors trauma and its repair as occurring in real life, not just as it appears in laboratory analysis.

Not only are the models valid, but equally important, they are predictably reproducible. Specifically, the PS model could be applied in PS scenarios to allow a customised design of surgery that best suits the individual in question.

In the analysis, we studied various plate shapes ranging from traditional linear plates to mesh pattern fixation plates. We also looked at various plate material ranging from titanium alloy (Ti-6Al-4V) to zirconia ( $ZrO_2$ ) and polylactic acid (PLA) and also in various dimensions.

With the analysis of these variants we found that whilst there were variations in performance between the various designs, they all performed equal to the physical parameters required for fracture fixation and subsequent repair. Across all variants of fixation methods, one significant factor is that the fractured ends of the bone are applied as closely as possible but not compressed.

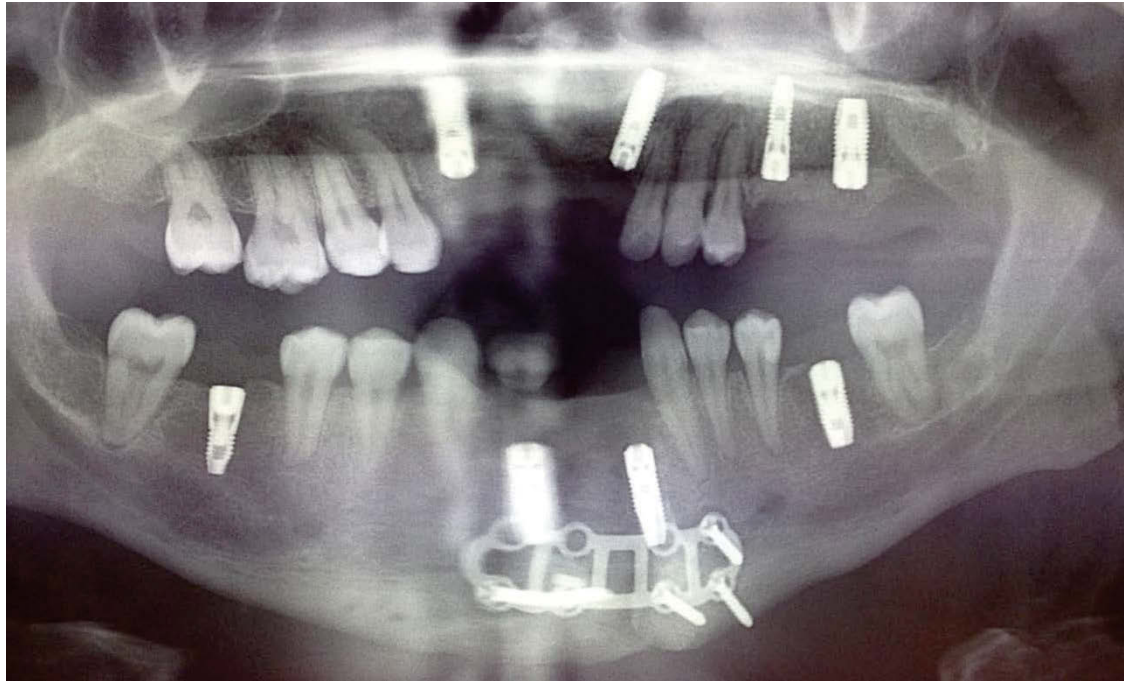


**Figure 0.1** Facial skeleton affected by congenitally associated tooth absence and neoplasia, requiring complex reconstruction with dental implants, grafting and fixation plate

The final product of this work is a reproducible valid model where production, performance and results represent a dialectic improvement over past mandibular models and which reproduces the most realistic scenario of constraints and forces during functional movements.

With further improvements, such as patient specific bone mineral density and the use of dedicated software for the manipulation of the computed tomography data, this model is destined to become a functional tool for clinical diagnosis and treatment in maxillofacial surgery and dentistry.

## ABBREVIATIONS

CBCT	cone beam computed tomography
CT	computed tomographic
EMG	electromyogram
FEA	finite element analysis
FEM	finite element model
FS	fracture segment
GEN	generic
IEMG	integrated electromyogram
IP	isolated plate
MRI	magnetic resonance image
PLA	polylactic acid
PS	patient specific
Ti	titanium
Ti-6Al-4V	titanium alloy
TMJ	temporomandibular joint
ZrO <sub>2</sub>	zirconium oxide (also known as zirconia)